Stabilization of a single-stranded DNA of adeno-associated virus by inverted terminal repeats

Yuan, Yuzhe ; Higashiyama, Kiyoko ; Ito-Kudo, Emi ; Masumi-Koizumi, Kyoko ; Yusa, Keisuke ; Uchida, Kazuhisa

(Citation)
Scientific Reports,14(1):27696

(Issue Date)
2024-11-12

(Resource Type)
journal article

(Version)
Version of Record

scientific reports

Check for updates

OPEN

Stabilization of a single-stranded DNA of adeno-associated virus by inverted terminal repeats

Yuzhe Yuan, Kiyoko Higashiyama, Emi Ito-Kudo, Kyoko Masumi-Koizumi, Keisuke Yusa & Kazuhisa Uchida✉

Parvoviruses have evolved to possess a linear single-stranded DNA (ssDNA) genome ranging from 4 to 6.3 kb. Adeno-associated virus (AAV), a member of the Parvoviridae family, contains approximately 5 kb of linear ssDNA within its capsid. This ssDNA features two 145-base inverted terminal repeats (ITRs) positioned at each end. ITRs have a T-shaped hairpin secondary structure, which plays a crucial role in viral replication. To investigate the impact of ITRs on ssDNA stability, we conducted a DNA denaturation-reannealing assay in 10 mM magnesium acetate, 50 mM potassium acetate, and 20 mM Tris-acetate buffer at pH7.9. Conventional double-stranded DNA (dsDNA) fragments retain a reannealing capability of over 50% for sizes under 8.8 kb, gradually losing this capability as sizes increase; however, dsDNA fragments in rAAV ranging from 0.7 to 6.3 kb did not exhibit a reannealing profile. This suggests that the presence of ITRs at both ends hinders annealing between the complementary strands. These results indicate that ITR structures preferentially induce an ssDNA conformation less than 6.3 kb in size, and that the stability of AAV ssDNA contributes to the viral life cycle, including processes such as infection, replication, and packaging. Considering the size of parvovirus genomes, it appears that their genomes require reversible flexibility in complementary DNA strands; simultaneously, this adaptability needs to be regulated by specific palindromic ITRs at both ends.

Keywords Adeno-associated virus, Single-stranded DNA, Inverted terminal repeat, Parvovirus

The family Parvoviridae is characterized by small non-enveloped viruses with linear, single-stranded DNA (ssDNA) genomes (4–6.3 kb) located within an icosahedral protein shell (23–28 nm in diameter)[1]. Parvoviruses infect a wide range of hosts from insects to primates[2,3] and include several significant mammalian pathogens such as erythroparvovirus B19, human bocavirus 1[4], feline parvovirus[5], canine parvovirus[6], and porcine parvovirus[7]. The presence of endogenous parvovirus sequences in the genomes of humans and other mammals suggests that parvoviruses were integrated into the germlines of diverse animal species at least 98 million years ago[8]. Typically, these viruses possess two major gene cassettes: one encodes a nonstructural protein (NS or Rep), which is essential for viral gene expression and DNA replication, and the other encodes the structural proteins of the capsid (CP or VP)[1]. However, some genera contain additional open reading frames (ORFs) adjacent to these genes or that overlap with alternative reading frames[9,10]. Linear- and single-stranded genomes exhibit specific secondary structures at their termini. The long coding region of 4–6.3 kb is flanked by short imperfect palindromes (116–550 nucleotides) that fold into the hairpin terminus. These hairpin sequences provide most of the cis-acting information required for DNA replication and packaging and give rise to viral replication origins when amplified through duplex replicative forms of DNA intermediates[11–13].

The most extensively studied parvoviruses are adeno-associated viruses (AAV), which are among the most commonly used viral vectors for gene therapy. The wild-type AAV genome is an ssDNA of approximately 4.7 kb enclosed within two 145-base inverted terminal repeats (ITRs)[14–17]. The ITR has been implicated as crucial in both the regulation and priming of AAV DNA replication[18,19], as well as other parvoviruses. AAV vectors for therapy are constructed by replacing viral genes with the gene of interest to be expressed in target cells, flanked by terminal ITR structures. Therefore, it is appropriate to analyze AAV vector DNA to evaluate the physical function of ITRs in ssDNA. In this study, we established a double-stranded DNA (dsDNA) denaturation-reannealing assay to examine the contribution of ITR structures to ssDNA stability and found that the presence of ITRs could stabilize ssDNA forms of less than 6.3 kb.

Graduate School of Science, Technology, and Innovation, Kobe University, 7-1-49 Minatojima Minamimachi, Chuo-ku, Kobe 650–0047, Japan. ✉email: kazuhisa.uchida@port.kobe-u.ac.jp

Results

Denaturation-reannealing assay for the evaluation of the stability of rAAV ssDNA

To assess the stability of ssDNA in recombinant AAV (rAAV), following digestion with PvuII and DraI to digest the plasmid DNA portion, we generated a double-stranded form of the 2.6-kb rAAV2-ZsGreen1 DNA from pAAV-ZsGreen1 (Fig. 1a, b). For the denaturation-reannealing assay, the digested DNA fragments were heat-treated ranging from 91 to 95 °C for 10 min, then gradually cooled to 25 °C at a ramp rate of -4 °C/min in 10 mM magnesium acetate, 50 mM potassium acetate, and 20 mM Tris-acetate buffer at pH 7.9 in the presence of 0.1 mg/ml bovine serum albumin (BSA). The samples were analyzed by electrophoresis using a TapeStation D5000 ScreenTape. As shown in Fig. 1c, the 5'- and 3'-termini of the ssDNA can form a T-shaped hairpin structure with double-stranded stems of 25 bases long, that are 15 bases shorter than those in rAAV DNA encapsulated in the vector capsid, the classical 40 bases of AAV2 wild type ITR. Specifically, the 15 bases of 5′-TT GGCCACTCCCTCT-3′ sequence is missing from the 5′-ITR, and the 5′-AGAGGGAGTGGCCAA-3′ sequence is missing from the 3′-ITR. The newly synthesized rAAV ITR is extended by 15 bases due to the DNA replication machinery (rolling circle replication)[1].

The calculated melting temperatures for the dsDNA fragments of 1.2, 0.94, and 0.69 kbp without ITRs were within the range of 84.1–84.3°C. In comparison to the control, denatured ssDNA was predominantly reannealed during the cooling process (Fig. 2a). The 1.2 kbp DNA could rehybridize with its complementary counterpart at a range of 68.8–79.5%, and similar results were obtained with other DNA fragments (0.11–0.94 kbp). However, the 2.6 kbp DNA did not denature at 90°C and 91°C for 10 min; instead, denaturation occurred in the double-stranded form from 93–96°C. During cooling to 25°C, the majority of the ssDNA failed to hybridize with its complementary counterpart. The reannealing rate of the 2.6 kb DNA was approximately 20% (Fig. 2b). The overall amount of DNA encompassing both single- and double-stranded forms was confirmed by denaturation using TapeStation RNA Screen Tape (Fig. 2a, lower panel), as described in our previous report[20]. These results indicated that > 80% of the 2.6 kb ssDNA of rAAV2-ZsGreen1 generated by heat treatment at temperatures exceeding 93°C for 10 min, did not reanneal and remained stable even after undergoing slow temperature reduction from 93°C to 25°C. Next, we performed a heat denaturation-reannealing assay using the rAAV DNA digested with PvuII/DraI/HindIII, PvuII/DraI/SphI, or PvuII/DraI/HindIII/SphI (Fig. 3a). HindIII digestion deleted the 5′-ITR, SphI deleted the 3′-ITR, and HindIII and SphI deleted both ITRs. The results clearly revealed that both ITRs are required to prevent reannealing (Fig. 3b, upper panel). It was also confirmed that the overall amount of DNA did not change following heat treatment and reannealing (Fig. 3b, lower panel). These results suggested that the formation of the 5′- and 3′-ITR T-shaped hairpin structure physically prevents the reannealing of complementary ssDNA by hindering the proximity of the 5' and 3' ends of the ssDNA.

Confirmation of the single-stranded form by ddPCR

To confirm the presence of ssDNA after heat treatment and reannealing, we compared the ZsGreen1 copy numbers with and without pretreatment using droplet digital PCR (ddPCR) (Table 1). When ssDNA was present independently in the reaction mixture, it was encapsulated in the droplets, resulting in a theoretical copy number for the ssDNA template that was two-fold higher than that of dsDNA. As illustrated in Fig. 2, approximately 80% of rAAV2-ZsGreen1 DNA adopted a single-stranded form, whereas 20% of the template DNA reannealed in a double-stranded form. This indicated that the copy number of rAAV after pretreatment was expected to be 1.8 times higher than that of the template without pretreatment. Indeed, rAAV2-ZsGreen1 showed a 1.76 times higher copy number after pretreatment than before (Table 1).

In the absence of both ITRs, or either the 5'-ITR or 3'-ITR, the ratio of copy numbers before and after pretreatment ranged from 0.86 to 1.03. These results suggest that heat treatment denatured the dsDNA structure and ssDNA was successfully reannealed. These findings support the idea that the formation of hybridized dsDNA requires stable annealing of the two-stranded termini. Additionally, when determining the AAV vector titer, it is important to carefully consider the condition of the ssDNA vector extracted from the capsids.

Confirmation of rAAV DNA form using DNA nucleases

To further confirm the presence of a single-stranded form of DNA after heat treatment and reannealing, we digested the DNA with DNases with different substrate specificities for single- and double-stranded forms and measured the copy number of the undigested template using ddPCR (Fig. 4). DNase I digests both dsDNA and ssDNA, with DNA-specific exonuclease activity acting in the 5' to 3' direction. Lambda exonuclease catalyzes the removal of nucleotides from the phosphorylated terminus of dsDNA in the 5' to 3' direction but has negligible activity on ssDNA. Nuclease P1 has single-stranded specific endonuclease activity against DNA, and nuclease activity against dsDNA was suppressed in 10 mM Bis-Tris-Propane-HCl and 10 mM $MgCl_2$, pH 7.0 (data not shown). Without denaturation-reannealing, the double-stranded form of rAAV2-ZsGreen1 DNA yielded 1×10^4 copies, whereas the template DNA (0.25 μg) was degraded by incubation of the mixture for 30 min at 37°C with 1 unit of DNase I (Fig. 4a, left). Similar results were obtained with the lambda exonuclease, which degrades most double-stranded templates. However, Nuclease P1 failed to digest the double-stranded template DNA. These results indicate that these DNA nucleases have substrate specificity. Conversely, heat treatment at 95°C for 10 min caused a significant alteration in substrate specificity for DNA nucleases (Fig. 4a, right). The rAAV DNA was no longer degraded by the lambda exonuclease and became susceptible to nuclease P1. These findings indicate that the lambda exonuclease no longer degrades the DNA because it remains stable in the ssDNA form after heat treatment/reannealing. Most PCR-targeting regions were single-stranded. Denatured DNA cannot revert to dsDNA because of the rapid formation of secondary structures in the ITR regions. ddPCR targeting the ITR yielded similar results without heat denaturation-reannealing (Fig. 4b, left). However, the copy number digested using lambda exonuclease was 39% of that of the control, suggesting that lambda exonuclease started to remove

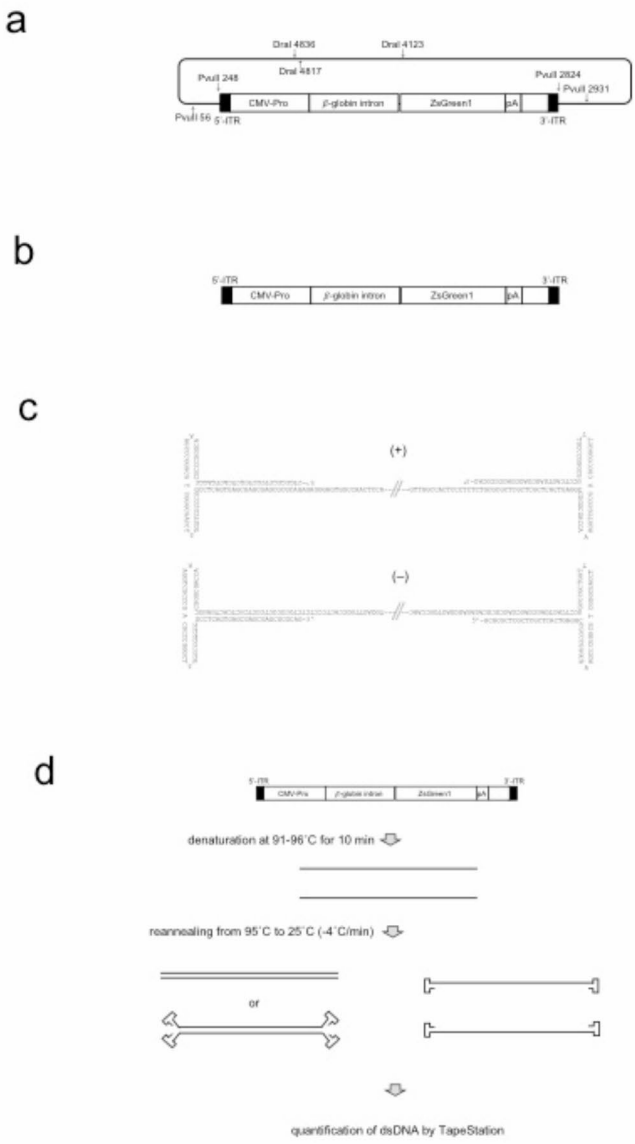

Fig. 1. Structure of pAAV-ZsGreen1, rAAV2-ZsGreen1 dsDNA, and rAAV2-ZsGreen1 ssDNA, and heat denaturation-reannealing assay. (**a**) pAAV-ZsGreen1 (5,716 bp) and digestion sites for PvuII and DraI. (**b**) rAAV2-ZsGreen1 dsDNA generated from pAAV-ZsGreen1 digested with PvuII. (**c**) ITR structures in rAAV2-ZsGreen1 ssDNA(+) and ssDNA(-). (**d**) heat denaturation-reannealing assay. dsDNA was heat denatured at 95 °C for 10 min, and cooled to 25 °C at -4 °C/min. The reannealed dsDNA was quantified by TapeStation. Total DNA was similarly confirmed by quantification of ssDNA by denaturing condition.

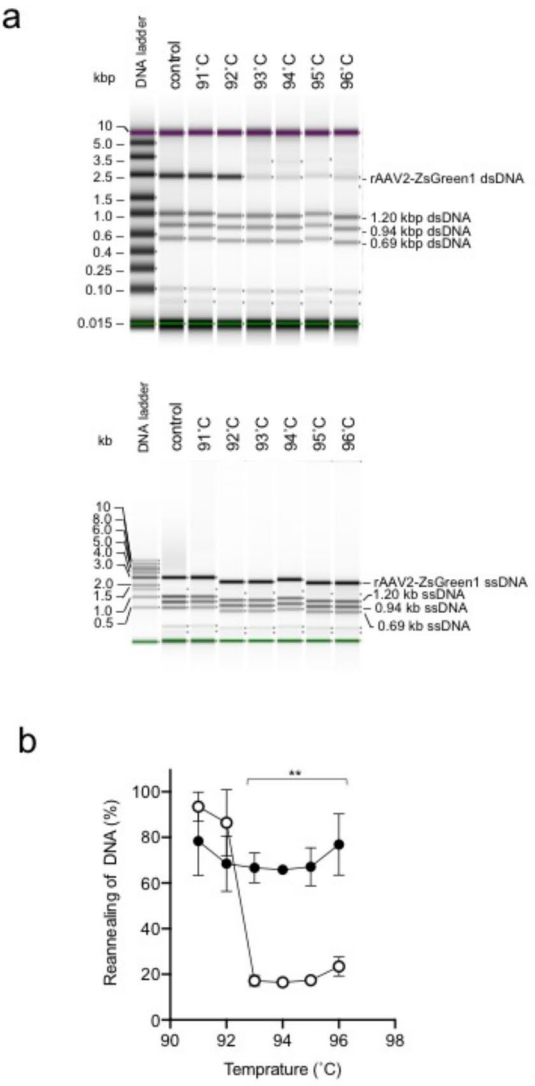

Fig. 2. Heat denaturation-reannealing assay of 2.6-kb rAAV2-ZsGreen1 dsDNA. (**a**) rAAV2-ZsGreen1 dsDNA generated from pAAV-ZsGreen1 digested with PvuII was heat-treated at 91, 92, 93, 94, 95, 96 °C for 10 min, and the temperature decreased to 25 °C at a -4 °C/min ramp rate. The dsDNA fragments after heat denaturation-reannealing were analyzed by TapeStation using D5000 ScreenTape (50 ng/μL) (upper panel). Similarly, the same samples were diluted 10-fold with TE buffer and analyzed using HS RNA ScreenTape (5 ng/μL) (lower panel). HS RNA ScreenTape (under denaturation condition) indicated the total amount of DNA in single-stranded form as a control. (**b**) dsDNA forms of 2.6-kb AAV-ZsGreen1 dsDNA (open circles) and 1.2-kb PvuII-DraI fragment (closed circles) as a control were plotted against denaturation temperature from 91–96 °C. The experiments were performed in triplicate, mean ± SD; * $p < 0.01$.

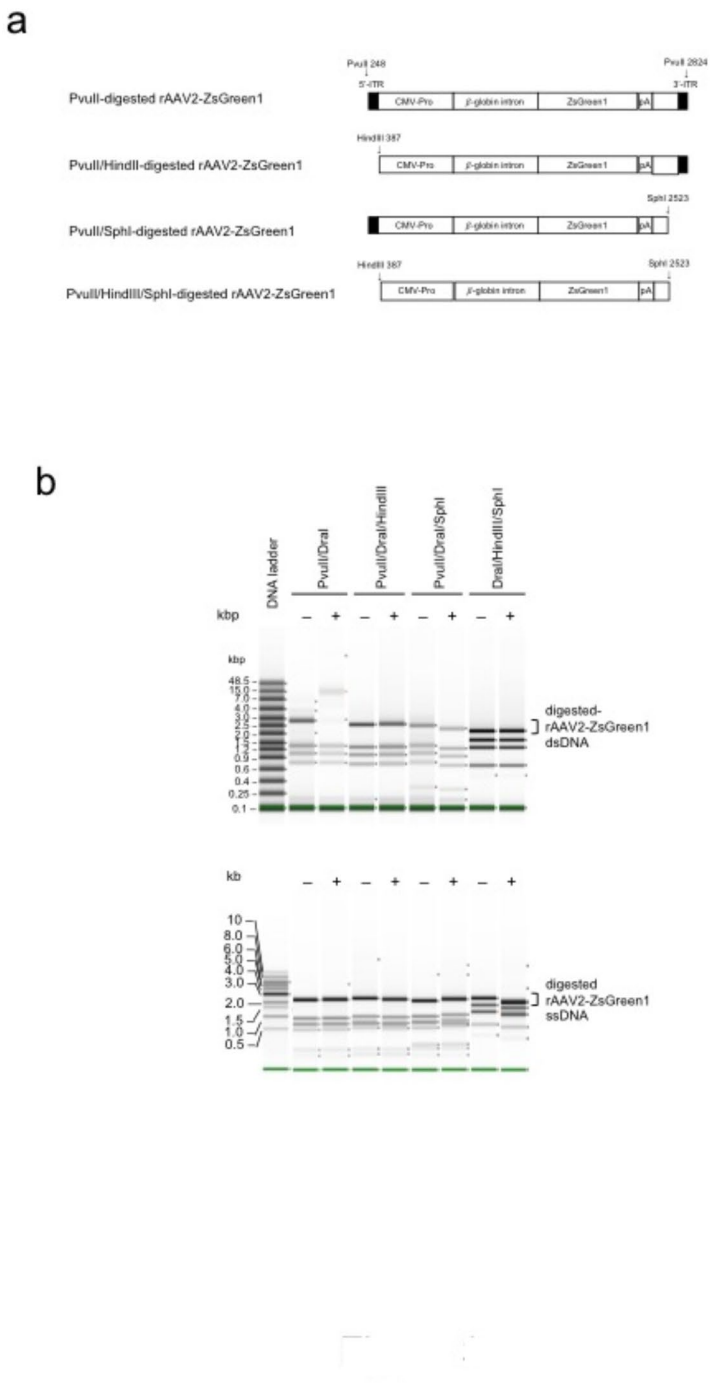

Fig. 3. Effect of ITRs on heat denaturation-reannealing assay of rAAV2-ZsGreen1 DNA. (**a**) Digestion sites of HindIII and SphI for rAAV2-ZsGreen1 DNA. (**b**) rAAV2-ZsGreen1 dsDNA with (+) or without (–) heat denaturation-reannealing treatment, after digestion of pAAV-ZsGreen1 with PvuII/DraI, PvuII/DraI/HindIII, PvuII/DraI/SphI, or PvuII/DraI/HindIII/SphI, were analyzed by TapeStation with Genomic ScreenTape (50 ng/μL) (upper panel). Similarly, the same samples were diluted 10-fold with TE buffer and analyzed using HS RNA ScreenTape (5 ng/μL) (lower panel). HS RNA ScreenTape indicated the total amount of DNA in single-stranded form as a control.

pAAV-ZsGreen1 digestion	Denaturation-reannealing	CPD[a]	Ratio (+/−)
PvuII	−	0.33 ± 0.02	1.76
	+	0.58 ± 0.01	
PvuII/HindIII	−	1.93 ± 0.03	0.89
	+	1.71 ± 0.03	
PvuII/SphI	−	0.22 ± 0.01	0.91
	+	0.20 ± 0.01	
PvuII/HindIII/SphI	−	0.34 ± 0.01	1.03
	+	0.35 ± 0.01	
PvuII/SmaI	−	0.28 ± 0	0.86
	+	0.24 ± 0	

Table 1. Copy number of rAAV2-ZsGreen1 DNA with or without denaturation-annealing. [a]The forward primer 5′-TTCGTGATCACCGGCGAGGGCAT-3′, reverse primer 5′-CCGTACATGAAGGCGGCGGACAA-3′, and probe [FAM]AACCTGTGCGTGGTGGAGGGCGGC[BHQ1] were used for ddPCR targeting ZsGreen1 in rAAV2 DNA (8,000 copies/reaction) without (−) or with (+) heat (95 °C, 10 min)–reannealing (95 °C to 25 °C at a ramp rate of -4 °C/min) before ddPCR.

nucleotides from the 5' terminus at the stem and completely degraded the 5'-ITR, even in the presence of three nucleotides without complementary nucleotides in the T-shaped terminal structure (Fig. 4b, right). Thus, the 3'-ITR was not digested by lambda exonuclease. Approximately 20% of rAAV DNA reverted to dsDNA after heat treatment and reannealing, as shown in Fig. 2b. However, 2.7% and 3.7% of rAAV DNA remained after treatment with nuclease P1, respectively, compared to the control. These results are inconsistent with those shown in Fig. 2b. These results suggested that a portion of the reannealed dsDNA, following denaturation, might contain partially unannealed nucleotides, making it susceptible to digestion by the single-stranded specific endonuclease.

Heat denaturation-reannealing assay for various sizes of DNA with or without ITRs

To evaluate the effect of DNA size on the heat denaturation-reannealing assay, linear DNA fragments of different sizes from pUC19 (2.7 kbp) and lambda phage DNA (48.5 kbp) were used. pUC19 DNA was digested with SmaI, PvuII, SmlI, or MlyI (Fig. 5a), and lambda phage DNA was digested with MluI, StuI, DraI, or PstI (Fig. 5b). The digested DNA fragments were subjected to the heat denaturation-reannealing assay. The DNA fragments (< 2.7 kb) generated from pUC19 exhibited high reannealing activity, regardless of the restriction enzyme used. Similarly, DNA fragments (< 5 kb) generated from lambda phage DNA were efficiently rehybridized with complementary DNA following heat denaturation. However, DNA fragments > 7–8 kb started to lose their annealing activity, and the 48.5 kb linear lambda phage DNA completely lost its ability to anneal. It is important to note that the 48.5 kbp linear DNA could be denatured at 95°C for 10 min, but no rehybridized dsDNA was detected after heat denaturation, indicating that rehybridization did not occur during the temperature descent period (from 95°C to 25°C) at a ramp rate of -4°C/min (Fig. 5b, lanes 1 and 2). The size of the DNA fragments was plotted against the reannealing rate to determine the overall profile of the DNA size in the heat denaturation/reannealing assay (Fig. 6). The profile revealed that conventional DNA fragments tend to lose their ability for rehybridization at approximately 7–9 kbp, indicating that it becomes challenging for ssDNA strands longer than 7–9 kb to retrace their path during the reannealing process when cooling from 95°C to 25°C at a ramp rate of -4°C/min. These data were used for a non-linear curve fitting analysis, and the fitting parameters were successfully obtained. To investigate how DNA length affects rAAV ssDNA stabilization by ITRs, we prepared pAAV-ZsGreen1 carrying stuffer DNA of 0.6–3.8 kbp at the SphI-BglII site and cleaved the rAAV2-ZsGreen1-stuffer DNA fragments (3.2–6.2 kbp) using PvuII digestion (Supplementary Fig. 1). Shorter rAAV2-ZsGreen1 DNA fragments (0.7, 1.0, and 1.9 kbp) were obtained from the deletion plasmids (Supplementary Fig. 2). Heat denaturation-reannealing assays were conducted similarly using these rAAV2-ZsGreen1 with stuffer or deletion (Fig. 5c, d). In contrast to conventional DNA fragments, ITRs suppressed rAAV ssDNA reannealing, as shown in Fig. 6. The 0.7–6.3 kbp dsDNA with ITRs could reanneal to a similar level (around 20%) as the 2.6 kbp rAAV2-ZsGreen1 DNA (Fig. 2). These results indicated that 0.7–6.3 kbp DNA without ITRs could rehybridize and revert to dsDNA, but the presence of ITRs could regulate the rehybridization activity, allowing it to function as a viral single-stranded genome. These results also suggest that the reannealing of both the 5' and 3' ends of complementary DNA strands is crucial for the stable formation of a double-stranded structure.

Discussion

Parvoviruses are relatively small viruses with a linear ssDNA genome of either negative or positive polarity, ranging from 4–6.3 kb. In this study, the reannealing rate of DNA after heat denaturation was analyzed using an automated electrophoresis system. Using this assay, we investigated the effect of the ITR structure of rAAV on ssDNA stabilization. The ≤ 8.8 kb ssDNA prepared from pUC19 and lambda phage DNA revealed that ≥ 50% of the ssDNA could reanneal, whereas the similarly sized ssDNA possessing ITRs at the ends did not show reannealing activity (Fig. 6). These results highlight the importance of stable hydrogen bonding at the 3' and 5'-termini of DNA in stable complementary strand hybridization for the reannealing process of ≤ 8.8 kb DNA.

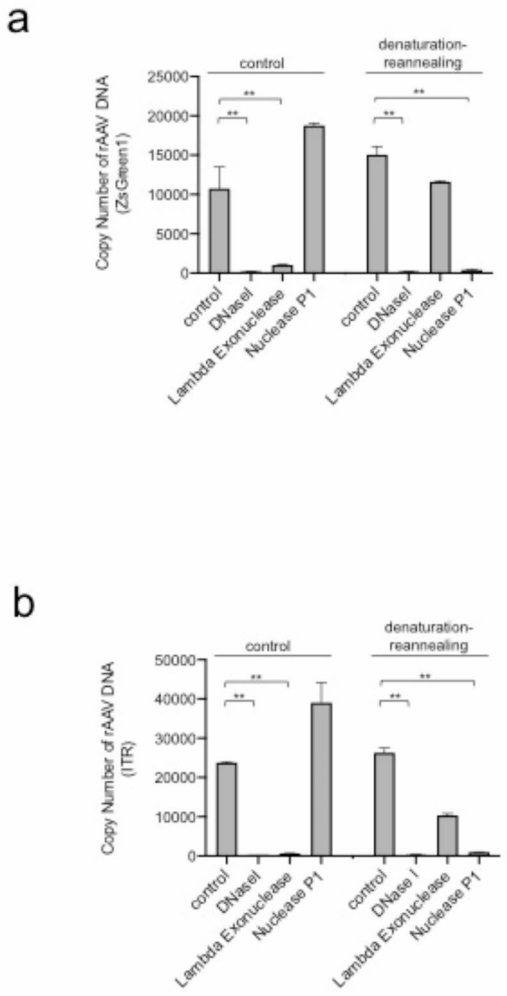

Fig. 4. DNase susceptibility of rAAV2-ZsGreen1 DNA following heat denaturation and reannealing. (**a**) rAAV2-ZsGreen1 dsDNA (1 µg pAAV-ZsGreen1 digested with PvuII/DraI) with (+) or without (–) denaturation-reannealing treatment was digested with DNase I (1 unit), lambda exonuclease (5 unit), or Nuclease P1 (100 unit) at 37 °C for 30 min, and the copy number of undigested rAAV DNA determined by ddPCR targeting ZsGreen1 (a) or ITR (**b**). The experiments were performed in triplicate, mean ± SD; ** $p < 0.01$.

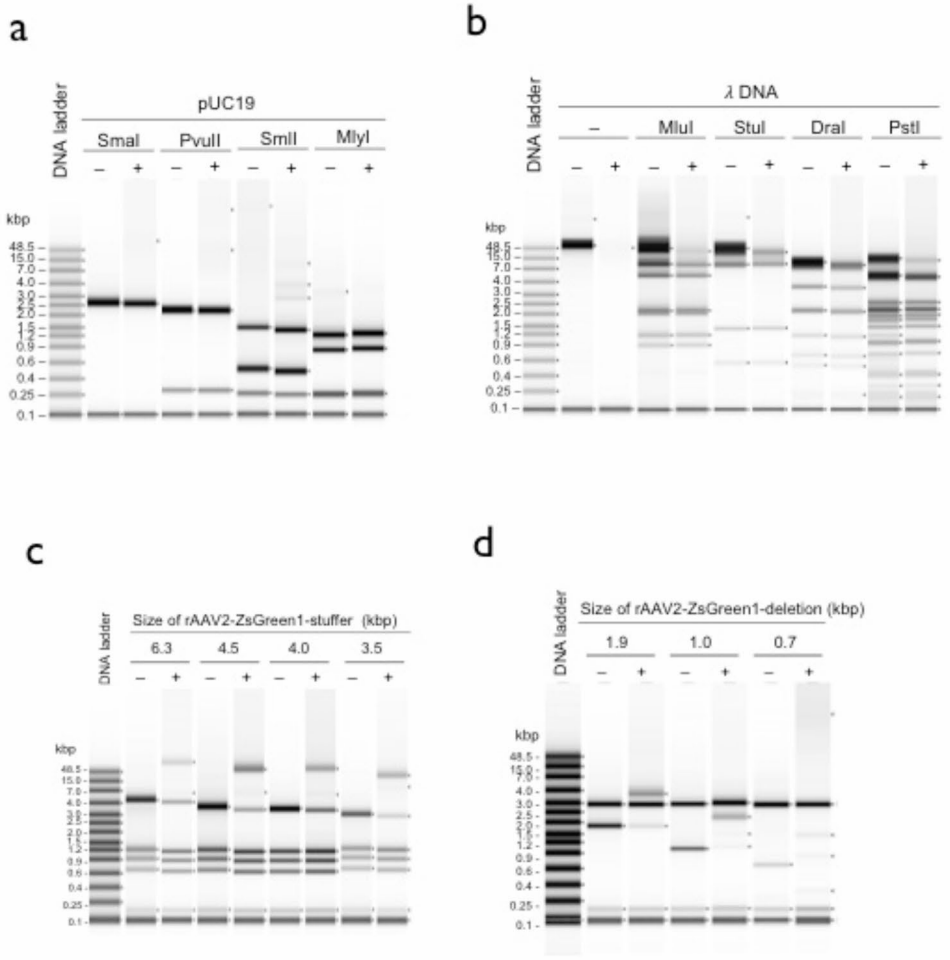

Fig. 5. Heat denaturation and reannealing of lambda and pUC19 DNA. (**a**) pUC19 DNA (0.5 µg) digested with 1 unit of *SmaI*, *PvuII*, *SmlI*, or *MlyI* with (+) or without (–) denaturation-reannealing treatment was analyzed by TapeStation using Genomic DNA ScreenTape. (**b**) Lambda DNA (0.5 µg) digested with 1 unit of MluI, StuI, DraI, or PstI was analyzed with (+) or without (–) denaturation-reannealing treatment by TapeStation using Genomic DNA ScreenTape. (**c**) dsDNAs of rAAV2-ZsGreen1 dsDNA (6.3, 4.5, 4.0 and 3.5 kb), and rAAV2-ZsGreen1 DNA (2.6 kb) digested from the plasmids (supplemental Figure S1) were analyzed with (+) or without (–) denaturation-reannealingtreatment by TapeStation using Genomic DNA ScreenTape. (**d**) dsDNAs of rAAV2-ZsGreen1 dsDNA (1.9, 1.0 and 0.7 kb) digested from the deletion plasmids (supplemental Figure S2) were analyzed with (+) or without (–) denaturation-reannealing treatment by TapeStation using Genomic DNA ScreenTape.

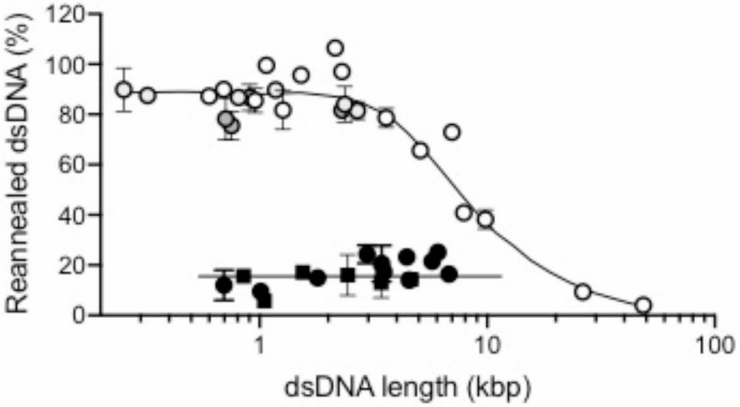

Fig. 6. Heat denaturation-reannealing assay of different size DNA fragments. The percentage of reannealed dsDNA following heat denaturation-reannealing was plotted against the size of the assayed DNA with (Fig. 5c, d, supplemental Figure S1-4a) or without ITRs (Fig. 5a, b, Figure S4b, c). Conventional dsDNA fragments from lambda DNA and pUC19 are indicated by open circles and gray-filled circles, respectively. Deletion mutants of rAAV2-ZsGreen1 and rAAV2-ZsGreen1 plus stuffer DNA are plotted in closed circles. rAAV-$\lambda_{0.41-4.63}$ with ITRs were in closed squares and rAAV-$\lambda_{0.41-4.63}$ without ITRs were in dark gray-filled circles. The fitted curve was obtained using R, n-parameter logistic regression; EC_{50}, 8.8; goodness of fit (GOF), 0.9276; and weighted GOF, 0.9992.

Wild-type AAV has a linear ssDNA of approximately 5 kb in size, which can be either positively or negatively oriented, and comprises two genes, known as Rep and Cap. This genetic structure is flanked by T-shaped ITRs[21]. AAV ITRs play a pivotal role in the processes of replication, encapsidation, and integration of the viral genome into the host genome[22]. Genome replication is initiated through the interaction of Rep78/68 with Rep-binding sites (RBE) and terminal resolution sites (trs) located within ITRs. The interaction of Rep78/68 with RBE triggers the synthesis of the second strand from the free 3'-OH end of the ITRs, while nicking in the trs sequence ensures ITR replication[23]. During encapsidation, Rep52/40 binds to the ITRs, facilitating the insertion of the AAV genome into the capsid due to its helicase activity[24]. Throughout these sequential replication events, ITRs may keep a newly synthesized ssDNA in a single-stranded form, contributing to the stability required for efficient replication and encapsidation within the capsids. In this report, the two AAV ITRs at the ends function to retain ssDNA stably by preventing single strands form reannealing.

Recent advances in metagenome sequencing targeting large viral populations in environmental samples have revealed an astonishing abundance of viromes in various habitats across the biosphere. Through metagenomic analysis of thousands of samples, the number of identified viral genes has increased approximately 16-fold[25,26].

Over 125,000 new viral genomes have been identified, and a significant proportion of these viral sequences belong to ssDNA viruses possessing circular or linear DNA genomes[8,27–31]. Virus families with circular ssDNA genomes represent rich diversity within the group of 13 virus families that possess ssDNA genomes, totaling 11 families. However, viruses with linear ssDNA genomes are limited to two families. Furthermore, their genome sizes appear to be confined to the range of 4–6.7 kb. In conventional DNA, ssDNA larger than 8.8 kb rapidly loses its ability to revert to dsDNA, conceivably forming DNA containing intramolecular secondary structures or incorrect intermolecular partial annealing, rather than successfully forming complete hybridization with complementary ssDNA (Fig. 6). One reason for the restriction of the parvovirus genome size to 4–6.3 kb may be the reannealing flexibility of ssDNA to revert to dsDNA. Simultaneously, parvoviruses may also need to control the annealing activity of ssDNA using ITRs.

Parvoviruses have downsized their own genome and opted for an ultra-small capsid structure measuring 25 nm, composed of 60 capsid protein molecules[1]. Downsizing offers advantages for viral survival, and also reduces the likelihood of detection by the immune system. In the pursuit of downsizing, this virus has adopted ssDNA for its genome. However, a challenge with ssDNA is that short ssDNA (4–6.3 kb) readily undergoes reannealing in the presence of Mg. This property is significant because of its implications in utilizing ssDNA as the viral genome; however, it is not inherently advantageous and requires control. For stabilization, during its evolutionary process, Parvoviruses were required to choose between two methods of ssDNA stabilization, both with different approaches. One involves acquiring proteins that stabilize ssDNA, whereas the other involves stabilizing ssDNA in its single-stranded form by introducing appropriate secondary structures. Parvoviruses choose the latter path and are believed to have acquired ITR structures at the 5' and 3' ends in AAV. This choice allowed parvoviruses to adopt a life cycle that stabilizes ssDNA as a secure genome within the capsid, achieved by packaging it with ITR structures, primarily for safeguarding its genetic information.

Methods

DNA and restriction enzymes

pAAV-ZsGreen1 (Takara Bio, cat#TKR6231), Lambda DNA (New England Biolabs, cat#N3011), and pUC19 (Nippon Gene, cat#311–01004) were used in this study. Plasmids were transformed into *Escherichia coli* (DH5α strain), and a single clone was then seeded in 25 ml of Terrific Broth (Thermo Fisher Scientific, cat#A1374301) containing 50 μg/mL ampicillin and cultured with shaking at 34 °C for 18 h. Plasmids were purified using the QIAGEN Plasmid Midi Kit (Qiagen, cat#12143). The purified plasmid was eluted in TE buffer (10 mM Tris-HCl and 1 mM EDTA, pH 7.5) and stored at 4 °C until use. For DNA quantification, the ultraviolet absorbance at 260 nm was measured using a NanoDrop spectrophotometer (Thermo Fisher Scientific). For digestion, 1 μg plasmid DNA was digested with 5 units of the restriction enzyme in 50 mM potassium acetate, 20 mM Tris acetic acid, 10 mM magnesium acetate, and 100 μg/mL BSA, pH 7.9. The restriction enzymes were purchased from New England Biolabs (USA). After restriction enzyme treatment, DraI (cat. #R0129), HindIII (cat. #R3104), MlyI (cat. #R0610), MluI (cat. # R3198), PstI (cat. #R3140), PvuII (cat. #R3151), SphI (cat. #R3182), SmlI (cat. #R0597) and StuI (cat. #R0187), SmaI (cat. #R0141), NdeI (cat. #R0111) were inactivated by heating at 65 °C for 20 min, NcoI (cat. #R3193) were inactivated at 80 °C for 20 min. While samples digested using BglII (cat. #R0144) and BamHI (cat. #R0136) were conducted AMPureXP beads purification without the heat-inactivation.

DNA heat denaturation-reannealing assay

The DNA fragment(s) (0.5–50 ng/mL) was transferred to two tubes of 20 μl each in 10 mM magnesium acetate, 50 mM potassium acetate, and 20 mM tris-acetate buffer at pH 7.9 in the presence of 0.1 mg/ml BSA, and one heated at 95 °C for 10 min and then cooled to 25 °C at a ramp rate of -4 °C/min. Subsequently, for < 5.0 kb DNA analysis, 1 μl each of the heated and unheated DNA fragment(s) were added into 10 μl of D5000 Sample Buffer (Agilent, cat. # 5067–5589), and analyzed using a TapeStation 4150 (Agilent) with a D5000 ScreenTape (Agilent, cat#5067–5588). For ≥ 5 kb DNA analysis, similarly 1 μl each of the heated and unheated DNA fragment(s) were added into 10 μl of Genomic DNA Sample Buffer (Agilent, cat. # 5067–5366), and analyzed using a TapeStation 4150 (Agilent) with a D5000 ScreenTape (Agilent, cat#5067–5365). For electrophoresis under denaturing conditions, the DNA fragments were 10-fold diluted with TE, and 4 μl of the diluted solution was added to an equal volume of High Sensitivity RNA Buffer (Agilent, cat. #5067–5580), heated at 72 °C for 5 min, and analyzed on a TapeStation 4150.

ddPCR

All primers and probes were custom-synthesized and HPLC-purified (Eurofins Genomics K.K, Tokyo, Japan). The forward primer 5′-TTCGTGATCACCGGCGAGGGCAT-3′, reverse primer 5′-CCGTACATGAAGGC GGCGGACAA-3′, and probe [FAM]AACCTGTGCGTGGTGGAGGGCGGC[BHQ1] were used for ddPCR targeting ZsGreen1. For ddPCR targeting ITR, the forward primer 5′-GGAACCCCTAGTGATGGAGTT-3′, and reverse primer 5′-CGGCCTCAGTGAGCGA-3′, and probe [FAM]CACTCCCTCTCTGCGCGCTC G[BHQ1] was used for ddPCR. For ddPCR, the reaction mixture was composed of 10 μL of ddPCR Supermix for Probes (No dUTP) (Bio-Rad Laboratories, Hercules, CA, USA), 2 μL of primers (final concentration of each primer was 0.9 μM), 1 μL of probe (final concentration, 0.25 μM), and 1 μL of the template diluted with TE buffer containing 0.01% PF-68 in a final volume of 20 μL. Each DNA template was tested in triplicate at two dilutions. The plates were then transferred to a QX200 Automated Droplet Generator (Bio-Rad Laboratories). A 96-well plate containing generated droplets was transferred to a C1000 Touch Thermal Cycler (Bio-Rad Laboratories). The cycling conditions were as follows: 10 min at 95 °C, followed by 40 cycles of a two-step thermal profile comprising 30 s at 94 °C and 60 s at 60 °C. The plate was then transferred to a QX200 droplet reader (Bio-Rad Laboratories) and the data were analyzed using QuantaSoft software (version 1.7.4.0917; Bio-Rad Laboratories).

The threshold separating the negative and positive droplets was manually set just above or below the cluster of negative and positive droplets, respectively.

DNase sensitivity assay

For DNase sensitivity assays, 0.1 µg of plasmid DNA, digested with restriction enzymes in 20 µL of buffer A (10 mM magnesium acetate, 50 mM potassium acetate in 20 mM Tris-acetate, pH 7.9), was either treated or untreated with denaturation-reannealing. The DNA sample (5 ng/µL) was digested with 1 unit of DNase I (Takara Bio, 2270 A), 5 units of Lambda exonuclease (New England Biolabs, M0262), or 100 units of Nuclease P1 (New England Biolabs, M0660) in the corresponding buffer. Reactions were terminated by adding 10 mM ethylenediaminetetraacetic acid (EDTA) and heating at 75 °C for 10 min. Copy numbers of ZsGreen1 or ITR were determined by ddPCR as described above.

Construction of pAAV-ZsGreen1 of different sizes

Oncorhynchus keta genomic DNA was digested using BglII and SphI, and the digested DNA was inserted into the plasmid pAAV-ZsGreen1, also digested with BglII and SphI. The ligated plasmids were transformed into *E. coli* (DH5alpha), inoculated onto an LB agar plate (100 µg/mL ampicillin), and seven clones carrying 0.4–3.6 kb stuffer DNA selected using PCR. The clones were further inoculated, and the stuffer DNA fragments of various sizes then amplified using primers with HindIII and SphI cleavage sequence tags attached to the 3'-end, digested with restriction enzymes, and then ligated to pAAV-ZsGreen1 to transform *E. coli* DH5α. After conversion, the *E. coli* were seeded on 1% agar/LB plates. The presence or absence of the stuffer DNA insertion plasmid was determined using 1% agarose gel electrophoresis after the plasmid was prepared and digested with HindIII and SphI. For construction of pAAV-ZsGreen1$\Delta_{0.7-1.9}$, pAAV-ZsGreen1 was digested with restriction enzymes of NcoI, NdeI and BamHI, and NdeI and SphI, respectively. Fragments of NcoI-NcoI (0.7 kb), NdeI-BamHI (1.0 kb), NdeI-SphI (1.9 kb) were removed from pAAV-ZsGreen1 structure. These fragment-deleted pAAV-ZsGreen1 were blunt-ended, self-ligated, and transformed into *E. coli* DH5α. These pAAV-ZsGreen1 deletion mutants were purified using QIAGEN Plasmid Midi Kit, and performed the downstream denaturation-reannealing assay.

Curve fitting of heat denaturation-reannealing assay

Non-linear curve fitting of DNA size versus reannealing rate was performed using R, n-parameter logistic regression.

Data availability

Data availabilityAll other datasets used or analyzed during the current study are available from the correspondingauthor on reasonable request.

Received: 19 March 2024; Accepted: 3 November 2024
Published online: 12 November 2024

References

1. Berns, K. & Parrish, C. *Parvoviridae* 7th edn, Vol. 2, 2437–2477 (Wolters Kluwer, 2007).
2. François, S. et al. Discovery of parvovirus-related sequences in an unexpected broad range of animals. *Sci. Rep.* **6**, 30880. https://doi.org/10.1038/srep30880 (2016).
3. Jager, M. C., Tomlinson, J. E., Lopez-Astacio, R. A. & Parrish, C. R. Van De Walle, G. R. Small but mighty: Old and new parvoviruses of veterinary significance. *Virol. J.* **18**, 210. https://doi.org/10.1186/s12985-021-01677-y (2021).
4. Qiu, J., Söderlund-Venermo, M. & Young, N. S. Human parvoviruses. *Clin. Microbiol. Rev.* **30**, 43–113. https://doi.org/10.1128/cmr.00040-16 (2017).
5. Stuetzer, B. & Hartmann, K. Feline parvovirus infection and associated diseases. *Vet. J.* **201**, 150–155. https://doi.org/10.1016/j.tvjl.2014.05.027 (2014).
6. Parrish, C. R. Pathogenesis of feline Panleukopenia virus and canine parvovirus. *Baillieres Clin. Haematol.* **8**, 57–71. https://doi.org/10.1016/s0950-3536(05)80232-x (1995).
7. Streck, A. F. & Truyen, U. Porcine parvovirus. *Curr. Issues Mol. Biol.* **37**, 33–46. https://doi.org/10.21775/cimb.037.033 (2020).
8. Liu, H. et al. Widespread endogenization of densoviruses and parvoviruses in animal and human genomes. *J. Virol.* **85**, 9863–9876. https://doi.org/10.1128/jvi.00828-11 (2011).
9. Ogden, P. J., Kelsic, E. D., Sinai, S. & Church, G. M. Comprehensive AAV capsid fitness landscape reveals a viral gene and enables machine-guided design. *Science*. **366**, 1139–1143. https://doi.org/10.1126/science.aaw2900 (2019).
10. Sonntag, F., Schmidt, K. & Kleinschmidt, J. A. A viral assembly factor promotes AAV2 capsid formation in the nucleolus. *Proc. Natl. Acad. Sci. U S A*. **107**, 10220–10225. https://doi.org/10.1073/pnas.1001673107 (2010).
11. Duan, D., Yan, Z., Yue, Y. & Engelhardt, J. F. Structural analysis of adeno-associated virus transduction circular intermediates. *Virology*. **261**, 8–14. https://doi.org/10.1006/viro.1999.9821 (1999).
12. Wilmott, P., Lisowski, L., Alexander, I. E. & Logan, G. J. A user's guide to the Inverted Terminal repeats of Adeno-Associated Virus. *Hum. Gene Ther. Methods*. **30**, 206–213. https://doi.org/10.1089/hgtb.2019.276 (2019).
13. Tai, P. W. L. & ITRs The terminal Frontier. *Hum. Gene Ther.* **31**, 143–144. https://doi.org/10.1089/hum.2020.29108.pwt (2020).
14. Berns, K. I. & Muzyczka, N. A. A. V. An overview of unanswered questions. *Hum. Gene Ther.* **28**, 308–313. https://doi.org/10.1089/hum.2017.048 (2017).
15. Earley, L. F. et al. Adeno-associated virus serotype-specific inverted terminal repeat sequence role in vector transgene expression. *Hum. Gene Ther.* **31**, 151–162. https://doi.org/10.1089/hum.2019.274 (2020).
16. Hirsch, M. L. Adeno-associated virus inverted terminal repeats stimulate gene editing. *Gene Ther.* **22**, 190–195. https://doi.org/10.1038/gt.2014.109 (2015).
17. Yan, Z., Zak, R., Zhang, Y. & Engelhardt, J. F. Inverted terminal repeat sequences are important for intermolecular recombination and circularization of adeno-associated virus genomes. *J. Virol.* **79**, 364–379. https://doi.org/10.1128/jvi.79.1.364-379.2005 (2005).
18. Hauswirth, W. W. & Berns, K. I. Origin and termination of adeno-associated virus DNA replication. *Virology*. **78**, 488–499. https://doi.org/10.1016/0042-6822(77)90125-8 (1977).

19. Srivastava, A. Replication of the adeno-associated virus DNA termini in vitro. *Intervirology*. **27**, 138–147. https://doi.org/10.1159/000149732 (1987).
20. Yuan, Y. et al. Concise analysis of single-stranded DNA of recombinant adeno-associated virus by automated electrophoresis system. *Hum. Gene Ther.* https://doi.org/10.1089/hum.2023.148 (2023).
21. Leonard, C. J. & Berns, K. I. Adeno-associated virus type 2: a latent life cycle. *Prog. Nucleic Acid Res. Mol. Biol.* **48**, 29–52. https://doi.org/10.1016/s0079-6603(08)60852-1 (1994).
22. Bennett, A., Mietzsch, M. & Agbandje-McKenna, M. Understanding capsid assembly and genome packaging for adeno-associated viruses. *Fut. Virol.* **12**, 283–297. https://doi.org/10.2217/fvl-2017-0011 (2017).
23. Bulliard, Y. et al. Structure-function analyses point to a polynucleotide-accommodating groove essential for APOBEC3A restriction activities. *J. Virol.* **85**, 1765–1776. https://doi.org/10.1128/jvi.01651-10 (2011).
24. Maurer, A. C. & Weitzman, M. D. Adeno-associated virus genome interactions important for vector production and transduction. *Hum. Gene Ther.* **31**, 499–511. https://doi.org/10.1089/hum.2020.069 (2020).
25. Suttle, C. A. Viruses: unlocking the greatest biodiversity on Earth. *Genome*. **56**, 542–544. https://doi.org/10.1139/gen-2013-0152 (2013).
26. Simmonds, P. et al. Consensus statement: Virus taxonomy in the age of metagenomics. *Nat. Rev. Microbiol.* **15**, 161–168. https://doi.org/10.1038/nrmicro.2016.177 (2017).
27. Krupovic, M. & Forterre, P. Single-stranded DNA viruses employ a variety of mechanisms for integration into host genomes. *Ann. N Y Acad. Sci.* **1341**, 41–53. https://doi.org/10.1111/nyas.12675 (2015).
28. Kryukov, K., Ueda, M. T., Imanishi, T. & Nakagawa, S. Systematic survey of non-retroviral virus-like elements in eukaryotic genomes. *Virus Res.* **262**, 30–36. https://doi.org/10.1016/j.virusres.2018.02.002 (2019).
29. Rosario, K., Duffy, S. & Breitbart, M. A field guide to eukaryotic circular single-stranded DNA viruses: insights gained from metagenomics. *Arch. Virol.* **157**, 1851–1871. https://doi.org/10.1007/s00705-012-1391-y (2012).
30. Zhao, L., Rosario, K., Breitbart, M. & Duffy, S. Eukaryotic circular Rep-Encoding single-stranded DNA (CRESS DNA) viruses: ubiquitous viruses with small genomes and a diverse host range. *Adv. Virus Res.* **103**, 71–133. https://doi.org/10.1016/bs.aivir.2018.10.001 (2019).
31. Malathi, V. G. & Renuka Devi, P. ssDNA viruses: key players in global virome. *Virusdisease*. **30**, 3–12. https://doi.org/10.1007/s13337-019-00519-4 (2019).

Acknowledgements

This work was funded by AMED under the grant numbers JP18ae0201001 and JP18ae0201002.

Author contributions

Y.Y., K.Y., and K.U. designed the study, and Y.Y., K.H., E.I.K., and K.M.K. performed the experiments. Y.Y., K.Y., and K.U. wrote the manuscript. All the authors have read and approved the final manuscript.

Declarations

Competing interests

The author declares no competing interests.

Additional information

Supplementary Information The online version contains supplementary material available at https://doi.org/10.1038/s41598-024-78612-y.

Correspondence and requests for materials should be addressed to K.U.

Reprints and permissions information is available at www.nature.com/reprints.

Publisher's note Springer Nature remains neutral with regard to jurisdictional claims in published maps and institutional affiliations.